Neoplasia 43 (2023) 100921

Contents lists available at ScienceDirect

Neoplasia

journal homepage: www.elsevier.com/locate/neo

Original Research

Therapeutic HDAC inhibition in hypermutant diffuse intrinsic pontine glioma

Alyssa Noll [a,b,c], Carrie Myers [a,b], Matthew C. Biery [a,b], Michael Meechan [a], Sophie Tahiri [a,d], Asmitha Rajendran [a,e], Michael E. Berens [f], Danyelle Paine [f], Sara Byron [g], Jiaming Zhang [g], Conrad Winter [b], Fiona Pakiam [b], Sarah E.S. Leary [a,b,h], Bonnie L. Cole [i,j], Evangeline R. Jackson [k,l], Matthew D. Dun [k,l,m], Jessica B. Foster [n,o], Myron K. Evans [a,h], Siobhan S. Pattwell [a,h], James M. Olson [a,b,h], Nicholas A. Vitanza [a,b,h,j,*]

[a] *Ben Towne Center for Childhood Cancer Research, Seattle Children's Research Institute, Seattle, WA, USA*
[b] *Clinical Research Division, Fred Hutchinson Cancer Center, Seattle, WA, USA*
[c] *Molecular and Cellular Biology Graduate Program and Medical Scientist Training Program, University of Washington, Seattle, WA, USA*
[d] *Molecular Mechanisms of Disease Graduate Program, University of Washington, Seattle, WA, USA*
[e] *Biomedical Informatics and Medical Education Graduate Program, University of Washington, Seattle, WA, USA*
[f] *Cancer & Cell Biology Division, Translational Genomics Research Institute (TGen), Phoenix, AZ, USA*
[g] *Integrated Cancer Genomics Division, Translational Genomics Research Institute (TGen), Phoenix, AZ, USA*
[h] *Department of Pediatrics, Seattle Children's Hospital, University of Washington, Seattle, WA, USA*
[i] *Department of Laboratories, Seattle Children's Hospital, Seattle, WA, USA*
[j] *Department of Laboratory Medicine and Pathology, University of Washington School of Medicine, Seattle, WA, USA*
[k] *Cancer Signalling Research Group, School of Biomedical Sciences and Pharmacy, College of Health, Medicine and Wellbeing, University of Newcastle, Callaghan, NSW, Australia*
[l] *Precision Medicine Research Program, Hunter Medical Research Institute, New Lambton Heights, NSW, Australia*
[m] *Paediatric Program, Mark Hughes Foundation Centre for Brain Cancer Research, College of Health, Medicine and Wellbeing, University of Newcastle, Callaghan, NSW, Australia*
[n] *Division of Oncology, The Children's Hospital of Philadelphia, Philidelphia, PA, USA*
[o] *Department of Pediatrics, Perelman School of Medicine, University of Pennsylvania, Philadelphia, PA, USA*

ARTICLE INFO

Keywords:
Diffuse intrinsic pontine glioma (DIPG)
Hypermutant
Mismatch-repair (MMR)
Histone deacetylase inhibitor (HDACi)
Quisinostat

ABSTRACT

Constitutional mismatch repair deficiency (CMMRD) is a cancer predisposition syndrome associated with the development of hypermutant pediatric high-grade glioma, and confers a poor prognosis. While therapeutic histone deacetylase (HDAC) inhibition of diffuse intrinsic pontine glioma (DIPG) has been reported; here, we use a clinically relevant biopsy-derived hypermutant DIPG model (PBT-24FH) and a CRISPR-Cas9 induced genetic model to evaluate the efficacy of HDAC inhibition against hypermutant DIPG. We screened PBT-24FH cells for sensitivity to a panel of HDAC inhibitors (HDACis) *in vitro*, identifying two HDACis associated with low nanomolar IC50s, quisinostat (27 nM) and romidepsin (2 nM). *In vivo*, quisinostat proved more efficacious, inducing near-complete tumor regression in a PBT-24FH flank model. RNA sequencing revealed significant quisinostat-driven changes in gene expression, including upregulation of neural and pro-inflammatory genes. To validate the observed potency of quisinostat *in vivo* against additional hypermutant DIPG models, we tested quisinostat in genetically-induced mismatch repair (MMR)-deficient DIPG flank tumors, demonstrating that loss of MMR function increases sensitivity to quisinostat *in vivo*. Here, we establish the preclinical efficacy of quisinostat against hypermutant DIPG, supporting further investigation of epigenetic targeting of hypermutant pediatric

Abbreviations: Constitutional Mismatch Repair Deficiency, (CMMRD); diffuse intrinsic pontine glioma, (DIPG); histone deacetylase inhibitor, (HDACi); mismatch-repair, (MMR); tumor mutational burden, (TMB).

* Corresponding author at: Department of Pediatrics, Seattle Children's Hospital, University of Washington, M/S JMB-8, 1900 9th Avenue, Seattle, WA 98101, USA.

E-mail address: nicholas.vitanza@seattlechildrens.org (N.A. Vitanza).

https://doi.org/10.1016/j.neo.2023.100921
Received 16 March 2023; Received in revised form 28 July 2023; Accepted 2 August 2023

cancers with the potential for clinical translation. These findings support further investigation of HDAC inhibitors against pontine high-grade gliomas, beyond only those with histone mutations, as well as against other hypermutant central nervous system tumors.

Introduction

While outcomes for many pediatric cancers have improved over the past decades, pediatric high-grade glioma (pHGG), continues to be associated with dismal survival [1,2]. Diffuse intrinsic pontine glioma (DIPG) is an aggressive pHGG that arises in the ventral pons, with an average overall survival post-diagnosis of only 11 months [3]. 85% of DIPG tumors harbor K27M mutations in genes encoding histone 3 (H3) [4]. Following the discovery that other midline pHGG share this recurrent histone mutation, H3 K27M mutant DIPG has since been reclassified as diffuse midline glioma (DMG) [5]. In this manuscript, we will use the term DIPG to collectively refer to both H3 wildtype (WT) and H3 K27M mutant diffuse pontine glioma.

While pHGG are often characterized by significant genomic alterations that influence clinical outcomes, such as histone H3 variants or single gene fusion events [5–8],comprehensive genomic analyses have demonstrated that the number of somatic mutations in pHGG is significantly lower than that of adult HGG [9,10]. It is estimated that around 6% of pHGG are classified as hypermutant [11,12], defined as a tumor mutational burden (TMB) of >10 mutations per megabase. This represents a distinct subgroup with a unique pathogenesis and clinicopathological characteristics.

While in adult HGG, hypermutation commonly arises at the time of recurrence as a consequence of treatment with alkylating agents [13–15], in children, hypermutation is present at the time of diagnosis and likely influences initial response to therapy. These children classically carry germline mutations in DNA mismatch repair (MMR) genes, including *PMS2, MSH2, MSH6*, and *MLH1,* which drive an accumulation of somatic mutations and microsatellite instability [4,9,11,16]. In some cases, tumors acquire secondary somatic mutations in DNA polymerase (*POLE, POLD1*), leading to ultra-hypermutation (>100 mutations/megabase) [16,17]. Biallelic germline loss of MMR function leads to constitutional mismatch repair-deficiency (CMMRD), a highly penetrant cancer predisposition syndrome. It is estimated that nearly half of children with CMMRD will develop gliomas (average age 9.5 years) [18]. These children face a extremely poor prognosis, with a median survival post-relapse of 2.6 months [16,19]. Currently, treatment for hypermutant pHGG involves maximum surgical resection followed by focal radiation. As significant resection is not possible for diffuse gliomas in the pons and given that children with CMMRD are at high risk for secondary malignancies, there is a dire need for new therapies for hypermutant DIPG. While clinical trials of non-central nervous system (CNS) solid tumors have established high tumor mutational burden as a biomarker predicting improved clinical response to immune checkpoint blockade [20], this approach has not been as successful against hypermutant adult HGG. Checkpoint inhibitors have shown promise against hypermutant pHGG [16,21–24]; however, immune checkpoint blockade may not be sufficient monotherapy to improve clinical outcomes against such an aggressive, heterogenous disease [25].

Decades of clinical trials have cemented that DIPG tumors are unresponsive to conventional targeted therapies and chemotherapies such as temozolomide [26]. Consequently, the current standard of care for DIPG treatment is limited to focal radiation therapy, which delays disease progression for 3 months [5]. Since the identification of the H3 K27M histone mutations in the majority of DIPG tumors, a growing body of preclinical evidence suggests that epigenetic targeting of DIPG through HDAC inhibitors may be a promising treatment strategy. Histone deacetylases (HDACs) are enzymes that catalyze the removal of acetyl groups from lysine residues on the tails of histone proteins, thereby regulating gene expression. Inhibition of HDAC function induces significant changes in transcription and have demonstrated efficacy against H3 K27M mutant DIPG [27,28]. However, the efficacy of HDAC inhibitors (HDACis) may not be dependent on the presence of histone mutations. In fact, preclinical work investigating the utility of the HDACi panobinostat demonstrated potency against both H3K27M mutant and histone 3 wild-type (H3 WT) DIPG [27]. Thus, HDACis may be effective against other transcriptionally aberrant tumors. Here, we report the preclinical efficacy of the HDACis quisinostat and romidepsin against biopsy-derived treatment-naïve and adapted hypermutant DIPG models.

Materials and methods

Histology

Tumor sections were cut at 6 μm, mounted on positively charged slides (Fisherbrand, Cat#2155015). IHC slides were stained using a Ventana Discovery Ultra IHC/ISH auto-stainer. After a deparaffinization step, antigen retrieval was performed with CC1 (Roche-Ventana, Cat#950-500) for 32 min (37 °C). After blocking, sections were incubated with one of the following primary antibodies for 40 min at 37 °C: anti-Ki-67 (Cell Signaling, Cat#9027S), anti-CD276/B7-H3 (LS Bio, Cat#LS-C743430). Detection was accomplished with an anti-rabbit HQ/anti-HQ-HRP system (Roche-Ventana, Cat#760-4815 and #760-4820) paired with ChromoMap DAB kit (Roche-Ventana, Cat#760-159) and counterstained with hematoxylin and bluing solution. The slides were then dehydrated, cleared, and mounted with conventional coverslips for assessment with a brightfield microscope.

Human specimens and patient-derived cell cultures

Human cell cultures were generated with informed consent in compliance with Institutional Review Board (IRB) approval at Seattle Children's Hospital (#14449). For PBT-24FH, tumor tissue was obtained at Seattle Children's Hospital and cell cultures were created at Fred Hutchinson Cancer Center (FHCC) as described [28,29]. Cells were maintained in NeuroCult NS-A Basal Medium with NS-A Proliferation Supplement (STEMCELL Technologies), 1X Glutamax (ThermoFisher Scientific), 40 ng/mL epidermal growth factor (PeproTech), and 40 ng/mL fibroblast growth factor (PeproTech). 7316-212A cells were generously shared by the Children's Brain Tumor Network (CBTN). VUMC-DIPG-10 cells were generously shared by Dr. Esther Hulleman (VU University Medical Center, Amsterdam, The Netherlands). All cell culture models were validated by DNA fingerprinting.

Cell viability and apoptosis assays

Quisinostat (JNJ-26481585) and romidepsin (FK228) were purchased from Selleckchem. To assess cell viability, cells were plated in 96-well plates at 15,000 cells per well and cultured in the presence of drug or DMSO in triplicate. Experiments were repeated for validation. Cell viability was assessed after 24, 48, and 72 h using CellTiter-Glo® Luminescent Cell Viability Assay (Promega). Data was collected on a Synergy 2 plate reader (Bio-Tek). Cell viabilities were normalized to DMSO control values.

Two methods were utilized to evaluate apoptosis. PBT-24FH cells were plated in 6-well plates at 1×10^6 cells per well and cultured in the presence of DMSO or drug in duplicate. After 72 h, cells were collected and stained with Annexin V-FITC and DAPI (Biolegend) and analyzed using a Novocyte Flow Cytometer (ACEA Biosciences). Collected data

was analyzed using FlowJo software (Becton–Dickinson). To evaluate changes in caspase-3/7 expression, 5000 PBT-24FH cells were plated in 96-well plates and co-incubated with Incucyte Caspase-3/7 Green Dye (Sartorius) and either DMSO or drug. Apoptotic cells were quantified using the Incucyte SX5 cell analysis system (Sartorius) every 4 h. At each timepoint, caspase 3/7 expression was normalized to respective DMSO controls.

Western blotting

Cells were lysed in RIPA lysis buffer (ThermoFisher), supplemented with PhosSTOP and cOmplete inhibitors (Sigma-Aldrich). Protein concentrations were measured utilizing the Pierce BCA Protein Assay (ThermoFisher). Samples were resolved on Bolt 4–12% Bis-Tris gels (ThermoFisher) and transferred to 0.2 μm nitrocellulose. Membranes were blocked in a 5% BSA/TBS-T solution for 1 h and then incubated with the following primary antibodies in blocking solution for 24 h at 4 °C: anti-GAPDH (1:2500), Cell Signaling, Cat#97166S), anti-β-Actin (1:5000, Cell Signaling, Cat#3700S), Histone H3 (acetyl K9, K14, K18, K23, K27) (1:1000, Abcam, Cat#ab47915), anti-PMS2 (1:1000, Abcam, Cat#ab11068), anti-MSH2 (1:1000, Cell Signaling, Cat#2017S), or anti-cleaved PARP (1:500, Cell Signaling, Cat#9541S). Secondary antibodies were used at 1:10,000 (Li-Cor IRDye 800CW Donkey anti-Mouse IgG and IRDye 680RD Goat anti-Rabbit IgG, Cat#926-32212 and Cat#926-68071, respectively).

Surgical procedure and in vivo treatment of tumor bearing mice

PBT-24FH *in vivo* studies were conducted in accordance with Fred Hutchinson Cancer Center (FHCC) Institutional Animal Care and Use Committee (IACUC) approved protocol #1457. Female athymic nude (Hsd:Athymic Nude-Foxn1^{nu}) (Envigo) mice were injected subcutaneously in the right flank with ~2×10^6 dissociated PBT-24FH orthotopic xenograft tumor cells. Drugs were dissolved in 2% Tween80, 2% DMSO, 48% Peg300, 48% water, and dosed intraperitoneally (IP). Quisinostat was dosed at 10 mg/kg three times weekly, and romidepsin 1 mg/kg twice weekly [28]. Tumor volume was monitored using caliper measurements. Study endpoints included: 77 days on study, tumor burden of 1000 mm^3, or observation of acute drug-related toxicity. Tumor tissue was collected 24 h following the final dose of drug.

VUMC-DIPG-10 *in vivo* studies were conducted in accordance with SCRI IACUC approved protocol #ACUC00669. VUMC-DIPG-10 parental wild-type, *PMS2* KD and *MSH2* KD isogenic cell lines were implanted subcutaneously into soft tissue flank of female athymic nude mice at 2×10^6 cells per mouse in 20% matrigel. Once tumors reached approximately 100 mm^3, mice were enrolled on study and dosed with IP vehicle or quisinostat as previously described. Study endpoints included tumor size of 1000 mm^3, 60 days on study, or tumor ulceration. No drug related toxicity was observed. Differences in tumor burden across experimental groups were analyzed using unpaired welch's t tests.

Whole-genome sequencing

DNA was isolated from patient-derived DIPG cultures and from matched peripheral blood mononuclear cells (PBMCs) using the Quick-DNA extraction kit (Zymo Research). Whole genome sequencing (WGS) libraries were generated using the ThruPLEX DNA-Seq kit (Rubicon Genomics) or the KAPA Hyper Prep kit (KAPA Biosystems). Sequencing was performed on an Illumina NovaSeq6000 instrument. The mean target coverage for tumor cell lines was 25.4X (range across samples, 19-30X) and the mean target coverage for the peripheral blood samples was 8.8X (range across samples, 7-10X).

Somatic and germline variant analysis

WGS data was analyzed using the TGen phoenix pipeline (v1.2.0, https://github.com/tgen/phoenix/releases/tag/v1.2.0). Briefly, fastq files were aligned to the GRCh38 human reference genome using BWA. Copy number analysis was performed using GATK CNV. Somatic single nucleotide variants (SNVs) and small insertions and deletions (indels) were called using a consensus approach, requiring variants to be called by at least 3 of 4 variant callers (mutect2, octopus, strelka2, and vardict), with a minimum read depth of 10 required in both the tumor and normal sample. TMB was calculated using an in-house tool to report the total number of protein-coding SNVs and indels per callable megabase (Mb) from the tumor-normal analysis. Microsatellite instability (MSI) was assessed using MSIsensor (https://github.com/ding-lab/msisensor). Tumors with a MSIsensor score of 3.5 of greater were classified as being positive for microsatellite instability. Due to the low mean target coverage in the normal samples, tumor-only analysis was also performed with DeepVariant, filtering out variants called by DeepVariant in the paired normal sample, variants seen at a population allele frequency greater than 1%, and variants with a quality score lower than 25. Somatic variants were prioritized based on the gene being annotated as a Catalogue of Somatic Mutations in Cancer (COSMIC) cancer gene census gene or implicated in DIPG based on published literature [30]. Germline SNVs and small indels in the PBMC sample were called using DeepVariant, and pathogenic or likely-pathogenic germline variants in a selected panel of cancer predisposition genes were identified using ClinVar annotations (http://clinvar.com/).

RNA sequencing & expression analysis

PBT-24FH cells were treated in culture with quisinostat or DMSO for 72 h before total RNA isolation using the RNeasy Mini Kit (Qiagen #74104). All treatment conditions were collected in biological duplicate. Multiplexed RNA-Seq was performed on libraries generated using the TruSeq Stranded Total RNA Library Prep kit (Illumina) and sequenced on a NextSeq 2000 (Illumina). Resultant reads passing Illumina's quality threshold were aligned to hg38 using STAR v2.5.2a (2 pass mapping), counts per gene were generated using STAR2's internal quantification method, and log2 ratios of normalized data were calculated for vehicle treatment versus quisinostat treatments. Normalized log2(fold change) were utilized to identify top differentially expressed genes. For quantitative PCR, RNA was extracted and reverse transcribed to generate cDNA using Superscript IV reverse transcriptase (Life Technologies). mRNA expression of human *HTR3A*and *RNAse2* genes was quantified using Taqman probes (Life Technologies) on a QuantStudio 5 RT-PCR instrument (Applied Biosystems) using *ACTB* as a housekeeping control gene (Thermo Fisher).

Generation of Isogenic MMR-deficient VUMC-DIPG-10 cells

sgRNAs targeting PMS2 and MSH2 were designed using the Synthego CRISPR Gene KO design tool and purchased from Synthego (Supplemental Table 1). CRISPR-Cas9 editing was performed as described [31]. Nucleofection was performed using the 4D-Nucleofector TM X Unit (Lonza) using the program DS-120 and SF nucleofector solution. After 48 h, genomic DNA was extracted (Qiagen #69504). Genomic regions surrounding the CRISPR target genes were PCR amplified using Phusion Polymerase (Thermo Fisher). Following size verification by agarose gel electrophoresis, generated PCR products were column purified (Thermo Fisher #K310001) and submitted for Sanger sequencing (GeneWiz) using unique sequencing primers. See Supplemental Table 2.

Results

Whole exome sequencing and mutational frequencies across DIPG models

We previously described the establishment of treatment-naïve biopsy-derived DIPG cell cultures, genetically characterized using the UW-OncoPlex platform [28]. To investigate the genomic alterations of

these models in greater depth, we carried out whole-genome sequencing on tumor cultures and paired patient blood samples. Four cultures (PBT-14FH, PBT-22FH, PBT-27FH, PBT-09FH) carried the pathognomonic histone H3 mutation p.Lys27Met, including three *H3F3A* mutants and one *HIST1H3B* mutant (Fig. 1). Mutation frequencies across these four cultures were low (0.4–1.6 mutations per Mb), in concordance with published studies suggesting that H3 K27M mutant DIPG is mutationally quiet [9,17,32]. PBT-24FH, a H3 WT DIPG, was found to harbor biallelic germline mutations in the *PMS2* gene including a p.Arg578 frameshift loss of function mutation and a p.Arg578Cys single nucleotide variant of uncertain significance. In concordance with these findings, this patient had received a molecular pathologic diagnosis of constitutional mismatch repair deficiency (CMMRD) syndrome. Additional somatic mutations were identified including a heterozygous loss of function mutation in *MSH6* (p.Phe1088fs). Consistent with clinical testing, PBT-24FH was classified as hypermutant, with a tumor mutational burden of 12.9 mutations per Mb (Fig. 1). Correspondingly, PBT-24FH was the only culture found to harbor microsatellite instability, which is associated with defective DNA mismatch repair.

To further characterize the PBT-24FH genome, DNA copy number profiling was performed (Supplemental Fig. 1). Large scale chromosomal alternations were apparent, including loss of 9p, encompassing the genes *JAK2, CDKN2A/CDKN2B*, and *CD274/PD-L1*. In addition, gain of 15q and losses of chromosomes 21 and 22 were noted. Genomic copy number changes and structural variations in hypermutant pHGG are varied, ranging from a lack of copy number changes [17] to changes consistent with non-hypermutant DIPG [4,30]. Within the same patient, independent tumors have been shown to harbor distinct copy number profiles and somatic mutations [4], emphasizing the heterogeneity of the genetic changes that can be induced by germline mutations in MMR.

Quisinostat and romidepsin are effective against hypermutant DIPG at low nanomolar concentrations

HDAC inhibitors have been reported to induce cytotoxicity of DIPG cells by restoring H3 K27 methylation and normalizing oncogenic gene expression [27]. However, a growing body of literature suggests the anti-tumor effects of HDACis are mediated by additional mechanisms including modulation of miRNAs [33], alteration of protein kinase signaling [34], inhibition of off-target proteins [35], and interference with a cancer cell's ability to utilize acetate from chromatin [36].

We previously reported a screen of six HDACis against a panel of patient-derived DIPG cultures that identified quisinostat and romidepsin, two pan-HDAC inhibitors, as promising therapeutic agents [28]. To evaluate the efficacy of HDACis for hypermutant DIPG, we treated PBT-24FH cells with quisinostat or romidepsin and observed time and dose-dependent reductions in PBT-24FH viability (Fig. 2A). After 72 h, the IC_{50} of quisinostat and romidepsin were 27 nM and 2 nM, respectively. *In vitro* sensitivity to quisinostat and romidepsin was observed in an additional hypermutant pHGG model (*PMS2, POLE, ATRX, NF1* mutant) 7316-212A [37] (Supplemental Fig. 2A). Western blot analysis demonstrated dose-dependent increases in H3 acetylation and cleaved PARP following HDACi treatment, confirming on-target activity of the drugs (Supplemental Fig. 2B). Flow cytometry analysis of Annexin V and DAPI staining revealed dose-dependent increased cell death suggestive of apoptosis (Fig. 2B, Supplemental Fig. 2C). In addition,

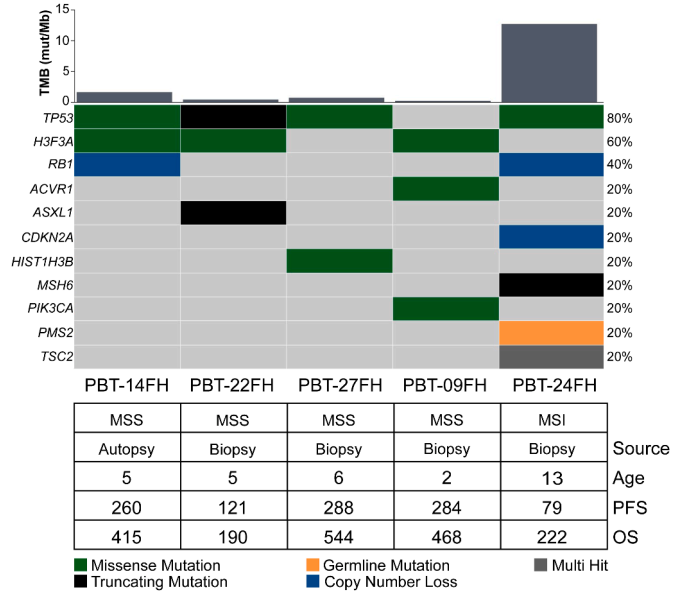

Fig. 1. Genomic analysis of a panel of patient-derived DIPG models. Clinicopathologic data for DIPG cultures is shown alongside corresponding tumor mutation rate, presence of microsatellite instability, and noted germline and somatic mutations. TMB, Tumor mutational burden; MSI, Microsatellite instability; MSS, Microsatellite stability; Age, Age at diagnosis in years; PFS, Progression Free Survival in days; OS, Overall Survival in days.

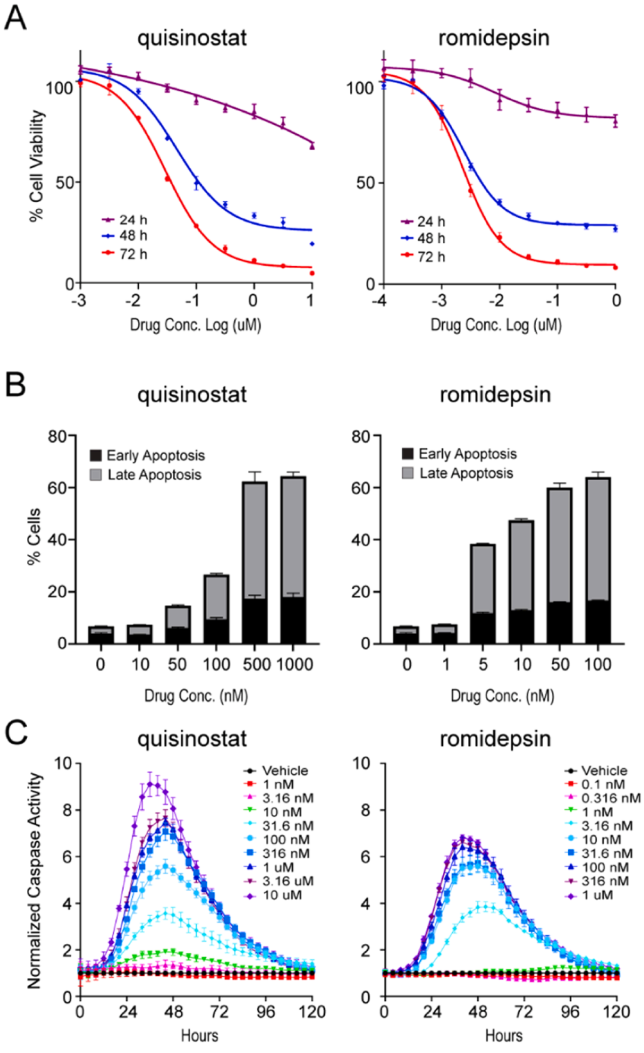

Fig. 2. Quisinostat and romidepsin exhibit low nanomolar efficacy against hypermutant DIPG. (A) Cell viability assay of PBT-24FH cells treated for 72 h with quisinostat or romidepsin at indicated concentrations or with DMSO. Data is shown as mean +/- SD. (B) Bar plots showing percentages of PBT-24FH cells undergoing early (Annexin V+ DAPI-) or late apoptosis (Annexin V+ DAPI+) following 72 h of drug treatment. Data is shown as mean +/- SD. (C) Expression of cleaved caspase 3/7 in PBT-24FH cells following 120 h of drug treatment. Data is shown as mean +/- SD.

dose-dependent increases in cleaved caspase 3/7 were observed (Fig. 2C), further supporting that quisinostat and romidepsin induce apoptosis of PBT-24FH cells *in vitro*.

Quisinostat significantly decreases tumor burden in a hypermutant DIPG flank model

Given that HDACis have limited penetration through the blood brain barrier [28], we next evaluated the efficacy of quisinostat and romidepsin in a PBT-24FH flank xenograft model. Tumor bearing mice were treated with intraperitoneal (IP) vehicle, quisinostat, or romidepsin. While mice in the vehicle and romidepsin groups underwent continued tumor growth, mice receiving quisinostat displayed near-complete tumor regression (Fig. 3A). 42 days following drug initiation, every vehicle-treated mouse had exited the study due to tumor burden (mean volume 940.4 mm^3). At this timepoint, the mean tumor volume of romidepsin-treated mice and quisinostat-treated mice was 669.1 mm^3 and 33.5 mm^3, respectively (Fig. 3B). No overt symptoms of toxicity (weight loss or behavioral changes) were observed in either treatment group (Supplemental Fig. 3). To further challenge the efficacy of quisinostat, two mice initially receiving romidepsin were switched to quisinostat treatment at a timepoint when they otherwise would have been removed from study due to tumor burden. In response, both mice displayed immediate and dramatic tumor regression (Fig. 3C). This observation highlights quisinostat's cytotoxic effect against both large tumors as well as a potential lack of cross-resistance between these two HDACis. Mice treated with quisinostat exhibited significantly prolonged survival ($p < 0.001$) compared to vehicle and romidepsin-treated groups (Fig. 3D). Examination of scant residual tumor foci by immunohistochemistry (IHC) revealed sparse hypertrophic, multi-nucleated tumor cells displaying a lower proliferative index present in quisinostat-treated mice (Fig. 3E).

Quisinostat induces broad transcriptomic changes in hypermutant DIPG

We next performed RNA sequencing (RNAseq) to analyze the transcriptomes of PBT-24FH cells treated with DMSO or a dose-titration of quisinostat (10 nM, 50 nM, 100 nM) for 72 h. The 20 most differentially expressed protein-coding genes are shown in Fig. 4A. Compared to DMSO, 10 nM quisinostat did not induce significant changes in gene expression. However, 50 and 100 nM of quisinostat mediated significant changes in gene transcription (Fig. 4B). Select transcriptomic changes identified in the RNAseq data were validated using quantitative RT-PCR (Fig. 4C). Next, we performed a gene ontology (GO) analysis on significantly upregulated protein-coding genes shared by the 50 nM and 100 nM samples (FDR < 0.01) (n = 1337). We found that quisinostat drove expression of genes associated with neuronal processes including synaptic vesicle clustering, calcium ion-regulated exocytosis of

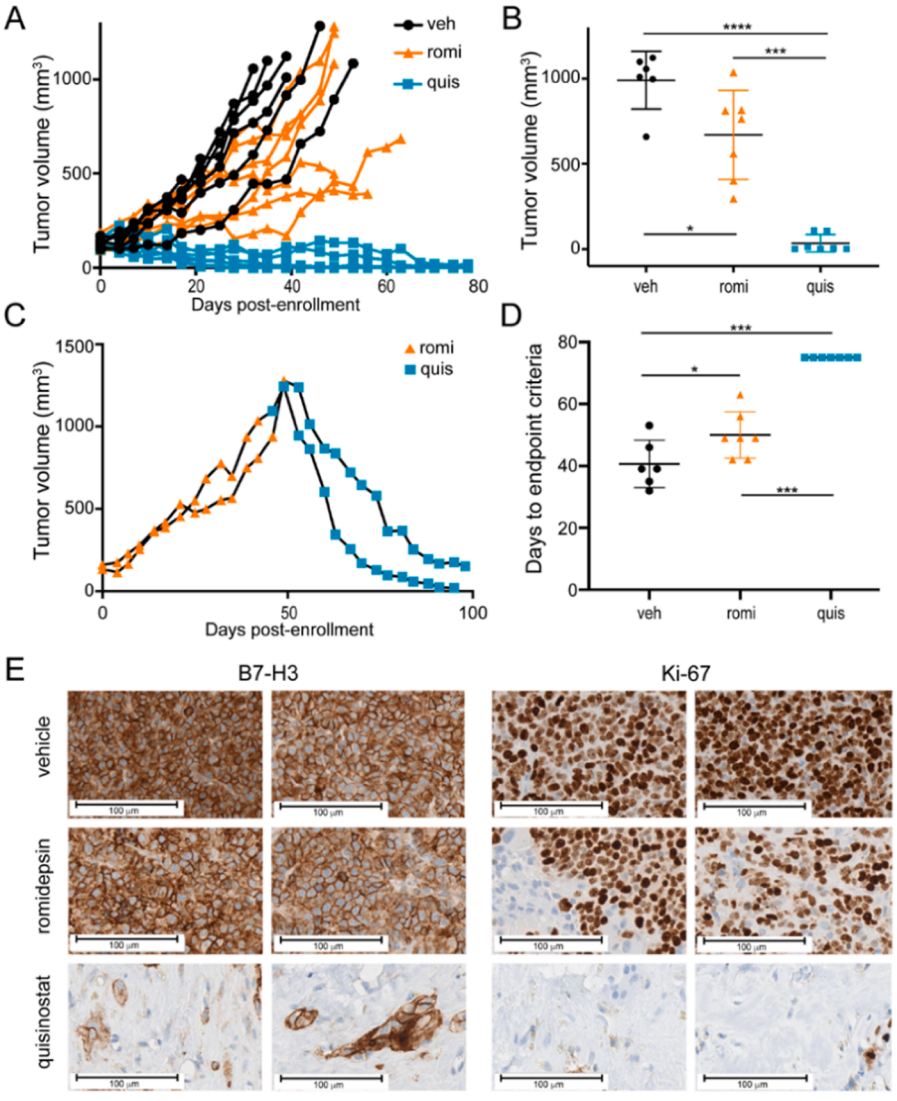

Fig. 3. Quisinostat significantly reduces tumor burden in an in vivo hypermutant flank model. (A) Tumor volume over time in PBT-24FH flank xenograft cohorts treated with systemic vehicle, quisinostat, or romidepsin. (B) Box plot displaying the average tumor volume of each cohort 42 days following drug initiation. Data is shown as mean +/- SD. (*$p < 0.05$, ***$p < 0.001$, ****$p < 0.0001$). (C) Volume of individual PBT-24FH flank tumors initially treated with romidepsin followed by a switch to quisinostat. (D) Box plot displaying the average number of days until study endpoint criteria were met in each cohort. Data is shown as mean +/- SD. (*$p < 0.05$, ***$p < 0.001$) (E) Immunohistochemistry of PBT-24FH tumors collected at study endpoints showing residual tumor cells (B7-H3+), and proliferative tumor cells (Ki-67+).

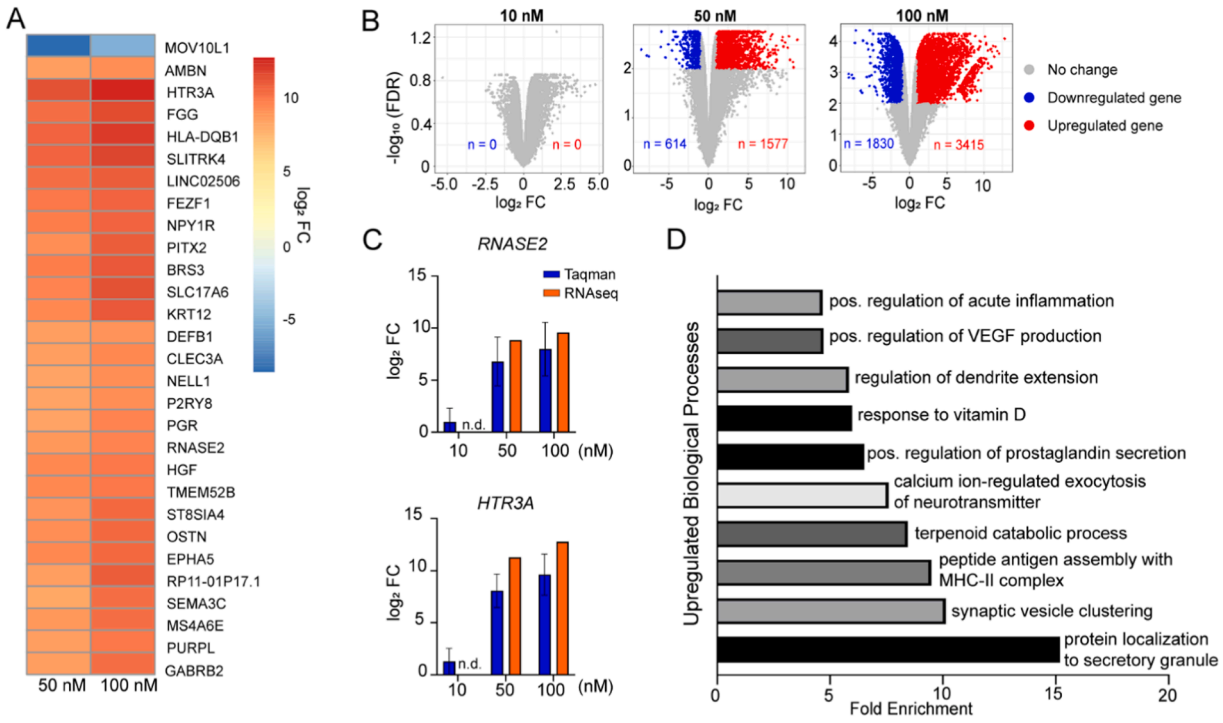

Fig. 4. Quisinostat-mediated transcriptional changes in PBT-24FH cells. (A) Heat map displaying Log_2(fold change) over DMSO vehicle control of the top 20 most differentially expressed genes (FDR < 0.01). (B) Volcano plots illustrating significantly differentially expressed genes (FDR < 0.01) induced by quisinostat (C) TaqMan PCR validation of expression changes in *HTR3A* and *RNASE2* compared to RNAseq results. (D) Gene Ontology biological processes associated with significantly upregulated genes shared by the 50 nM and 100 nM groups (FDR < 0.01). n.d, not detected.

neurotransmitter, and regulation of dendrite extension (Fig. 4D) (Supplemental Table 3). Additionally, quisinostat increased expression of genes associated with immune-related processes including antigen presentation with MHC-II, prostaglandin secretion, and acute inflammation. Additional genes involved in immune responses were identified including chemokines (*CXCL13*), cytokines (*IFNy, IL-1A, IL-1B, IL-6, IL-12A, IL-15, IL-18*), and costimulatory ligands (*CD40, CD70*) (Supplemental Table 3). Quisinostat was associated with a downregulation of genes mediating developmental processes including *NOTCH1, SOX8,* and *SOX9*, suggesting that quisinostat may downregulate expression of genes mediating neural stemness (Supplemental Table 3). Taken together, these transcriptional changes suggest that quisinostat promotes biological processes associated with neuronal differentiation and may promote a pro-inflammatory tumor microenvironment in hypermutant DIPG.

Quisinostat decreases tumor burden in a CRISPR induced mismatch repair-deficient DIPG model

Hypermutation in pHGG is commonly mediated by germline mutations in mismatch repair (MMR) genes. To evaluate the effect of MMR deficiency on sensitivity to quisinostat, *PMS2* and *MSH2* knock-down (KD) cell lines were generated of the H3 WT DIPG culture VUMC-DIPG-10 [38] using nucleofection of Cas9:sgRNA RNPs [31] (Supplemental Tables 1 and 2). Isogenic flank tumors were established, and tumor-bearing mice were treated with vehicle or quisinostat (Fig. 5A). No significant difference in tumor growth rate of vehicle-treated parental wild-type, *MSH2* KD, and *PMS2* KD flank tumors was observed ($p > 0.05$; Fig. 5B). After thirty days, quisinostat failed to significantly reduce parental tumor burden ($p > 0.05$; Fig. 5B). In contrast, quisinostat-treated *MSH2* KD and *PMS2* KD tumors exhibited a lower average tumor volume compared to their respective vehicle-treated group ($p < 0.001$, $p < 0.05$; Fig. 5B). Additionally, all 5 quisinostat-treated *MSH2* KD tumor-bearing mice remained healthy and on study at the pre-defined endpoint of 60 days, compared to parental (n = 3) and *PMS2* KD mice (n = 1) (Fig. 5C). To confirm that developed flank tumors retained loss of MMR protein, tumors were harvested at study endpoints and analyzed by Western blot. Results showed that established flank tumors retained an incomplete loss of MMR protein (Fig. 5D). These results suggest MMR function mediates sensitivity to quisinostat and indicates that sensitivity to quisinostat may be shared across MMR deficient hypermutant DIPG and other CNS tumors.

Discussion

It remains critical to establish effective therapies for DIPG, as overall survival has remained unchanged for decades despite powerful scientific discoveries [39]. DIPG clinical trials have failed to improve overall survival despite encouraging preclinical results, although future trials will hopefully incorporate lessons learned from clinically integrated next-generation sequencing and pharmaco-proteogenomic profiling [40, 41]. Preclinical studies have been limited by model systems that may be autopsy-derived with pretreatment that alters tumor biology and genetically-induced models that cannot account for the molecular heterogeneity even within a tumor subgroup such as DIPG. We have leveraged our clinical neurosurgical ability to biopsy tumors and quickly translate to treatment-naïve laboratory tumor cell lines. Using CRISPR technology, we also can combine patient-derived models with specific genetic introductions to further assess tumor subsets. This approach expands the relevance of preclinical findings specific to hypermutant DIPG tumors and should open investigations into the benefit of HDACis against other hypermutant CNS tumors.

Preclinical studies remain limited by the ability of HDACis to consistently traffic across the blood-brain barrier and into tumor, particularly into the pons and it is a limitation of this study to rely on flank model systems, though we believe this does support biological anti-tumor activity of the drug *in vivo*. The observed efficacy of quisinostat in this study further supports generation of blood-brain

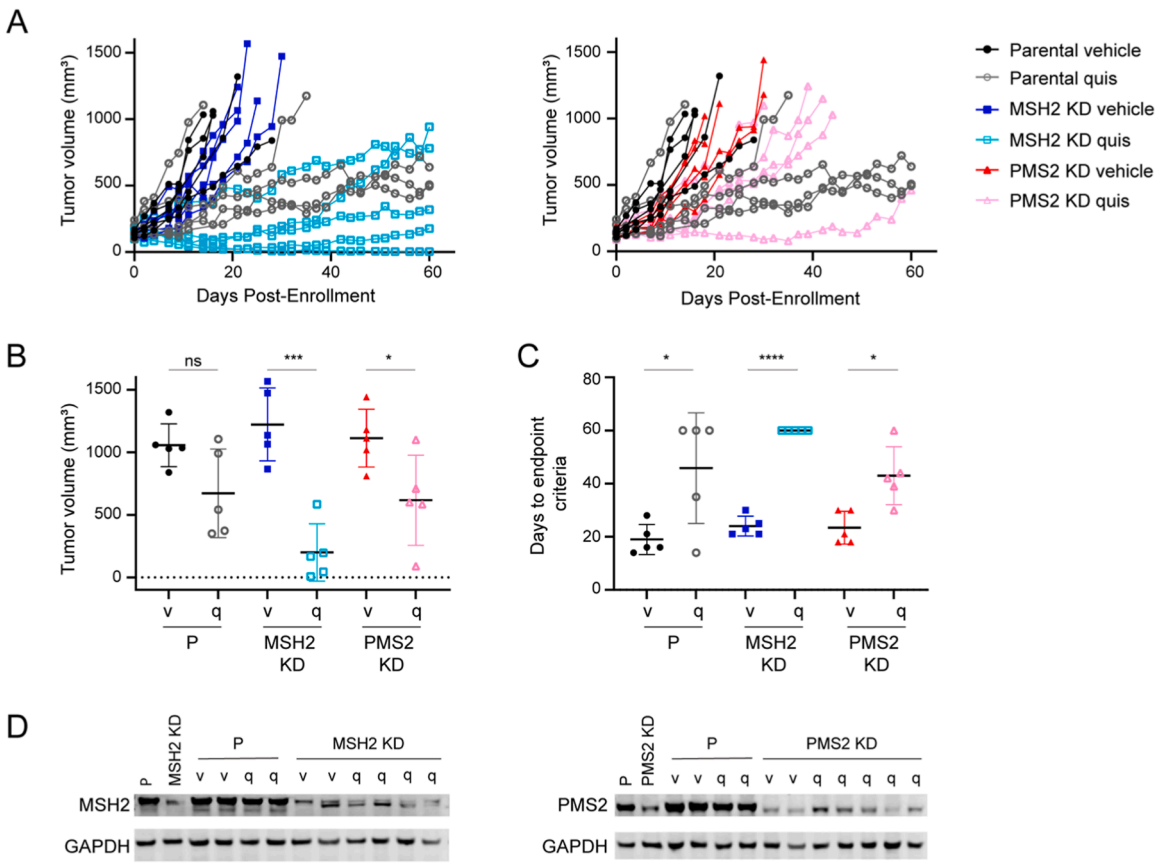

Fig. 5. Loss of MMR function induces sensitivity to quisinostat in vivo. (A) Tumor volume of VUMC-DIPG-10 isogenic flank xenograft cohorts over time treated with vehicle (v) or quisinostat (q). Each line is representative of a single mouse. (B) Box plot displaying the average tumor volume of each cohort thirty days following drug initiation (P, parental; ns, non-significant; *p <0.05, ***p < 0.001). (C) Box plot displaying the average number of days until study endpoint criteria were met by each cohort (*p <0.05, ****p < 0.0001). (D) Western blot displaying presence of MSH2 or PMS2 protein in VUMC-DIPG-10 cell lines or treated flank tumors.

penetrating versions of quisinostat as well as continued development of drug conjugates and enhanced locoregional delivery systems such as intra-ommaya approaches used in locoregional CAR T cell trials [42], intra-pontine approaches used in convention-enhanced delivery (CED) trials [43] or strategies to increase the permeability of the blood-brain barrier to enhance penetrance of HDACi [44]. Other preclinical work has shown benefit of blood brain barrier penetrant quisinostat [45,46] and hopefully can be preclinically evaluated in future orthotopic xenograft and genetically-induced models of DIPG.

While quisinostat has a low nanomolar IC_{50} *in vitro* and efficacy *in vivo*, the aggressive, heterogenous nature of malignant CNS tumors will limit its curative potential as a single agent [27]. Given HDACis have demonstrated potential as immunomodulators [47–49] and the documented responsiveness of hypermutant pHGG to immune checkpoint blockade [24], exploration of whether quisinostat and immunomodulatory agents may be effective in combination is warranted [25]. This strategy is supported by the observation that PBT-24FH upregulated several immune process genes including MHC Class II molecules, chemokines, cytokines, and co-stimulatory ligands in response to quisinostat. Additional studies are needed to evaluate the potential of quisinostat as a combinatorial agent for immunotherapy against hypermutant DIPG and other transcriptionally aberrant CNS tumors.

This study provides key insights into the design of clinical trials aiming to evaluate HDACis in pHGG. First, the striking anti-tumor effect of quisinostat observed in our PBT-24FH flank model supports the inclusion of H3 WT DIPG, including hypermutant DIPG, in clinical trials evaluating HDACis. HDACis are a diverse class of compounds, each with a unique selectivity for various HDACs. In this study, pre-treatment with romidepsin did not inhibit the anti-tumor effect of quisinostat *in vivo*, suggesting that previous treatment with an HDACi should not inherently serve as an exclusion criterion from another HDACi clinical trial. We advocate that biopsied pontine tumors receive an integrated molecular diagnosis which can identify relevant subgroups and in the case of histone wildtype tumors may uncover mutations associated with CMMRD syndrome. In summary, the data presented here supports the need for continued development of blood-brain-barrier penetrating quisinostat-like drugs for DIPG and provides valuable insight into HDACi clinical trial inclusion criteria.

Funding

We are grateful for generous support from The Andrew McDonough B+ Foundation, The Avery Huffman DIPG Foundation, Kristie and Joe Berg, Erin Cordry and Eric Hanson, Freckles from Heaven, the Julianna Sayler Foundation, The Kellen Joyce Heart of a Warrior Research Fund, Liv Like a Unicorn, Hope for Harlee Foundation, Live Gray's Way, Love for Lucy, the McKenna Claire Foundation, the Pediatric Brain Tumor Research Fund Guild of Seattle Children's, the Run of Hope Seattle, Sam Day Foundation, Starbucks, the Seattle Sounders, Team Beans Infant Brain Tumor Fund, Team Cozzi Foundation, Tommy Strong Foundation, and Unravel Pediatric Cancer, and We Love You Connie Foundation. Funding is also provided NIH grant R01CA114567 (J.M.O); Cookies for Kid's Cancer Young Investigator Grant (N.A.V.); DIPG All-In (N.A.V.); Matthew Larson Research Grant (N.A.V.); St. Baldrick's Stand Up to Cancer Dream Team Translational Cancer Research Grants (SU2C-AACR-DT-27-17 (N.A.V.), Stand Up to Cancer is a division of the Entertainment Industry Foundation and research grants are administered by the American Association for Cancer Research, the scientific

partner of SU2C).

CRediT authorship contribution statement

Alyssa Noll: Conceptualization, Data curation, Formal analysis, Investigation, Methodology, Project administration, Resources, Software, Validation, Visualization, Writing – original draft, Writing – review & editing. **Carrie Myers:** Data curation, Formal analysis, Investigation, Software, Writing – original draft, Writing – review & editing. **Matthew C. Biery:** Data curation, Writing – original draft, Formal analysis, Writing – review & editing, Investigation, Visualization, Resources, Validation, Software. **Michael Meechan:** Investigation, Software, Writing – review & editing. **Sophie Tahiri:** Investigation, Software, Writing – review & editing. **Asmitha Rajendran:** Investigation, Software, Writing – review & editing. **Michael E. Berens:** Formal analysis, Software, Validation, Writing – review & editing. **Danyelle Paine:** Formal analysis, Writing – review & editing, Investigation, Software. **Sara Byron:** Formal analysis, Software, Writing – review & editing. **Jiaming Zhang:** Formal analysis, Software, Writing – review & editing. **Conrad Winter:** Data curation, Writing – review & editing, Software. **Fiona Pakiam:** Data curation, Software, Writing – review & editing. **Sarah E.S. Leary:** Resources, Software, Writing – review & editing. **Bonnie L. Cole:** Resources, Software, Writing – review & editing. **Evangeline R. Jackson:** Investigation, Software, Writing – review & editing. **Matthew D. Dun:** Investigation, Software, Writing – original draft, Writing – review & editing. **Jessica B. Foster:** Investigation, Software, Methodology, Resources, Writing – review & editing. **Myron K. Evans:** Methodology, Software, Writing – review & editing. **Siobhan S. Pattwell:** Methodology, Software, Writing – review & editing. **James M. Olson:** Funding acquisition, Resources, Software, Supervision, Validation, Writing – review & editing. **Nicholas A. Vitanza:** Conceptualization, Funding acquisition, Methodology, Project administration, Software, Supervision, Validation, Writing – original draft, Writing – review & editing.

Declaration of Competing Interest

The authors declare that they have no known competing financial interests or personal relationships that could have appeared to influence the work reported in this paper.

Acknowledgments

We thank the children and families who bravely shoulder the burden of their disease and place their trust in Seattle Children's for their care. We thank our clinical team, including E. Crotty, A. Sato, R. Ronsley, C. Hoeppner, S. Holtzclaw, A. Wein, C. Anderson, O. Cook, A. Laurine, G. Mun, E. Stowe, C. Verda, W. Iwata, and C. Henson. We thank J. Stevens, the Seattle Children's Hospital's Department of Anatomic Pathology, and the TTS Brain Tumor Committee. Portions of the results previously have been presented (SNO, Boston, 2021; ISPNO, Hamburg, 2022).

Supplementary materials

Supplementary material associated with this article can be found, in the online version, at doi:10.1016/j.neo.2023.100921.

References

[1] S.C. Curtin, A.M. Minino, R.N. Anderson, Declines in cancer death rates among children and adolescents in the United States, 1999-2014, NCHS Data Brief 257 (2016) 1–8.
[2] Q.T. Ostrom, et al., CBTRUS statistical report: primary brain and other central nervous system tumors diagnosed in the United States in 2011-2015, Neuro-Oncology 20 (2018) iv1–iv86, https://doi.org/10.1093/neuonc/noy131.
[3] T. Cooney, et al., Contemporary survival endpoints: an international diffuse intrinsic pontine glioma registry study, Neuro-Oncology 19 (2017), https://doi.org/10.1093/neuonc/nox107.
[4] G. Wu, et al., The genomic landscape of diffuse intrinsic pontine glioma and pediatric non-brainstem high-grade glioma, Nat. Genet. 46 (2014) 444–450, https://doi.org/10.1038/ng.2938.
[5] N.A. Vitanza, M. Monje, Diffuse intrinsic pontine glioma: from diagnosis to next-generation clinical trials, Curr. Treat. Options Neurol. 21 (2019) 1–11, https://doi.org/10.1007/s11940-019-0577-y.
[6] D.A. Khuong-Quang, et al., K27M mutation in histone H3.3 defines clinically and biologically distinct subgroups of pediatric diffuse intrinsic pontine gliomas, Acta Neuropathol 124 (2012) 439–447, https://doi.org/10.1007/s00401-012-0998-0.
[7] G. Wu, et al., Somatic histone H3 alterations in pediatric diffuse intrinsic pontine gliomas and non-brainstem glioblastomas, Nat. Genet. 44 (2012) 251–253, https://doi.org/10.1038/ng.1102.
[8] J. Schwartzentruber, et al., Driver mutations in histone H3.3 and chromatin remodelling genes in paediatric glioblastoma, Nature 482 (2012) 226–231, https://doi.org/10.1038/nature10833.
[9] S.N. Gröbner, et al., The landscape of genomic alterations across childhood cancers, Nature 555 (2018) 321–327, https://doi.org/10.1038/nature25480.
[10] C. Jones, S.J. Baker, Unique genetic and epigenetic mechanisms driving paediatric diffuse high-grade glioma, Nat. Rev. Cancer 14 (2014) 651–661, https://doi.org/10.1038/nrc3811.
[11] A. Johnson, et al., Comprehensive genomic profiling of 282 pediatric low- and high-grade gliomas reveals genomic drivers, tumor mutational burden, and hypermutation signatures, Oncologist 22 (2017) 1478–1490, https://doi.org/10.1634/theoncologist.2017-0242.
[12] E.E. Crotty, et al., Children with DIPG and high-grade glioma treated with temozolomide, irinotecan, and bevacizumab: the Seattle Children's Hospital experience, J. Neurooncol. 148 (2020) 607–617, https://doi.org/10.1007/s11060-020-03558-w.
[13] M. Touat, et al., Mechanisms and therapeutic implications of hypermutation in gliomas, Nature 580 (2020) 517–523, https://doi.org/10.1038/s41586-020-2209-9.
[14] D.P. Cahill, et al., Loss of the mismatch repair protein MSH6 in human glioblastomas is associated with tumor progression during temozolomide treatment, Clin. Cancer Res. 13 (2007) 2038–2045, https://doi.org/10.1158/1078-0432.CCR-06-2149.
[15] C. Hunter, et al., A hypermutation phenotype and somatic MSH6 mutations in recurrent human malignant gliomas after alkylator chemotherapy, Cancer Res. 66 (2006) 3987–3991, https://doi.org/10.1158/0008-5472.CAN-06-0127.
[16] E. Bouffet, et al., Immune checkpoint inhibition for hypermutant glioblastoma multiforme resulting from germline biallelic mismatch repair deficiency, J. Clin. Oncol. 34 (2016) 2206–2211, https://doi.org/10.1200/JCO.2016.66.6552.
[17] A. Shlien, et al., Combined hereditary and somatic mutations of replication error repair genes result in rapid onset of ultra-hypermutated cancers, Nat. Genet. 47 (2015) 257–262, https://doi.org/10.1038/ng.3202.
[18] M. Abedalthagafi, Constitutional mismatch repair-deficiency: current problems and emerging therapeutic strategies, Oncotarget 9 (2018), https://doi.org/10.18632/oncotarget.26249.
[19] N. Amayiri, et al., High frequency of mismatch repair deficiency among pediatric high grade gliomas in Jordan, Int. J. Cancer 138 (2016) 380–385, https://doi.org/10.1002/ijc.29724.
[20] R.M. Samstein, et al., Tumor mutational load predicts survival after immunotherapy across multiple cancer types, Nat. Genet. 51 (2019) 202–206, https://doi.org/10.1038/s41588-018-0312-8.
[21] M. AlHarbi, et al., Durable response to nivolumab in a pediatric patient with refractory glioblastoma and constitutional biallelic mismatch repair deficiency, Oncologist 23 (2018) 1401–1406, https://doi.org/10.1634/theoncologist.2018-0163.
[22] V. Larouche, et al., Sustained complete response of recurrent glioblastoma to combined checkpoint inhibition in a young patient with constitutional mismatch repair deficiency, Pediatr. Blood Cancer 65 (2018), https://doi.org/10.1002/pbc.27389.
[23] C. Yang, et al., Lynch syndrome-associated ultra-hypermutated pediatric glioblastoma mimicking a constitutional mismatch repair deficiency syndrome, Cold Spring Harb. Mol. Case Stud. 5 (2019) a003863, https://doi.org/10.1101/mcs.a003863.
[24] A. Das, et al., Genomic predictors of response to PD-1 inhibition in children with germline DNA replication repair deficiency, Nat. Med. 28 (2022) 125–135, https://doi.org/10.1038/s41591-021-01581-6.
[25] M.L. Persson, et al., The intrinsic and microenvironmental features of diffuse midline glioma: implications for the development of effective immunotherapeutic treatment strategies, Neuro-Oncology 138 (2022) 380–385, https://doi.org/10.1093/neuonc/noac117.
[26] K.J. Cohen, et al., Temozolomide in the treatment of children with newly diagnosed diffuse intrinsic pontine gliomas: a report from the Children's Oncology Group, Neuro-oncology 13 (2011) 410–416, https://doi.org/10.1093/neuonc/noq205.
[27] C.S. Grasso, et al., Functionally defined therapeutic targets in diffuse intrinsic pontine glioma, Nat. Med. 21 (2015) 555–559, https://doi.org/10.1038/nm.3855.
[28] N.A. Vitanza, et al., Optimal therapeutic targeting by HDAC inhibition in biopsy-derived treatment-naïve diffuse midline glioma models, Neuro-Oncology 23 (2021) 376–386, https://doi.org/10.1093/neuonc/noaa249.
[29] M.C. Biery, et al., A protocol for the generation of treatment-naïve biopsy-derived diffuse intrinsic pontine glioma and diffuse midline glioma models, J. Exp. Neurol. 1 (2020) 158, https://doi.org/10.33696//Neurol.1.025.

[30] A. Mackay, et al., Integrated molecular meta-analysis of 1,000 pediatric high-grade and diffuse intrinsic pontine glioma, Cancer Cell 32 (2017) 520–537, https://doi.org/10.1016/j.ccell.2017.08.017.
[31] P. Hoellerbauer, et al., A simple and highly efficient method for multi-allelic CRISPR-Cas9 editing in primary cell cultures, Cancer Rep. (2020), https://doi.org/10.1002/cnr2.1269.
[32] K.R. Taylor, et al., Recurrent activating ACVR1 mutations in diffuse intrinsic pontine glioma, Nat. Genet. 46 (2014) 457–461, https://doi.org/10.1038/ng.2925.
[33] P. Autin, C. Blanquart, D. Fradin, Epigenetic drugs for cancer and microRNAs: a focus on histone deacetylase inhibitors, Cancers (Basel) 11 (2019) 1530, https://doi.org/10.3390/cancers11101530.
[34] C.S. Chen, S.C. Weng, P.H. Tseng, H.P. Lin, C.S. Chen, Histone acetylation-independent effect of histone deacetylase inhibitors on Akt through the reshuffling of protein phosphatase 1 complexes, J. Biol. Chem. 280 (2005) 38879–38887, https://doi.org/10.1074/jbc.M505733200.
[35] S. Lechner, et al., Target deconvolution of HDAC pharmacopoeia reveals MBLAC2 as common off-target, Nat. Chem. Biol. (2022), https://doi.org/10.1038/s41589-022-01015-5.
[36] S.R. Srivatsan, et al., Massively multiplex chemical transcriptomics at single-cell resolution, Science 367 (2020) 45–51, https://doi.org/10.1126/science.aax6234.
[37] H. Ijaz, et al., Pediatric high-grade glioma resources from the children's brain tumor tissue consortium, Neuro-Oncology 22 (2020) 163–165, https://doi.org/10.1093/neuonc/noz192.
[38] S. Nagaraja, et al., Transcriptional dependencies in diffuse intrinsic pontine glioma, Cancer Cell 31 (2017) 635–652, https://doi.org/10.1016/j.ccell.2017.03.011.
[39] T.B. Johung, M. Monje, Diffuse intrinsic pontine glioma: new pathophysiological insights and emerging therapeutic targets, Curr. Neuropharmacol. 15 (2017) 88–97, https://doi.org/10.2174/1570159x14666160509123229.
[40] D.S. Rogawski, N.A. Vitanza, A.C. Gauthier, V. Ramaswamy, C. Koschmann, Integrating RNA sequencing into neuro-oncology practice, Transl. Res. 189 (2017) 93–104, https://doi.org/10.1016/j.trsl.2017.06.013.
[41] I.J. Findlay, et al., Pharmaco-proteogenomic profiling of pediatric diffuse midline glioma to inform future treatment strategies, Oncogene 41 (2022) 461–475, https://doi.org/10.1038/s41388-021-02102-y.
[42] N.A. Vitanza, et al., Locoregional infusion of HER2-specific CAR T cells in children and young adults with recurrent or refractory CNS tumors: an interim analysis, Nat. Med. 27 (2021) 1544–1552, https://doi.org/10.1038/s41591-021-01404-8.
[43] M.M. Souweidane, et al., Convection-enhanced delivery for diffuse intrinsic pontine glioma: a single-centre, dose-escalation, phase 1 trial, Lancet Oncol. 19 (2018) 1040–1050, https://doi.org/10.1016/S1470-2045(18)30322-X.
[44] H.J. Wei, et al., Focused ultrasound-mediated blood-brain barrier opening enhances panobinostat efficacy in a murine diffuse intrinsic pontine glioma model, Int. J. Radiat. Oncol. Biol. Phys. 111 (2021), e177.
[45] K.T. Householder, et al., pH driven precipitation of quisinostat onto PLA-PEG nanoparticles enables treatment of intracranial glioblastoma, Colloids Surf. B Biointerfaces 166 (2018) 37–44, https://doi.org/10.1016/j.colsurfb.2018.02.048.
[46] M.H. Marand, E. Han, S.H. Kim, P.T. Hammond, J.P. Straehla, SURG-03. Layer-by-layer core-shell nanoparticles for the delivery of HDAC inhibitors to the central nervous system, Neuro-Oncology 25 (2023) i72, https://doi.org/10.1093/neuonc/noad073.279.
[47] X. Wang, et al., HDAC inhibitors overcome immunotherapy resistance in B-cell lymphoma, Protein Cell 11 (2020) 472–482, https://doi.org/10.1007/s13238-020-00694-x.
[48] T. Sun, et al., Histone deacetylase inhibition up-regulates MHC class I to facilitate cytotoxic T lymphocyte-mediated tumor cell killing in glioma cells, J. Cancer 10 (2019) 5638–5645, https://doi.org/10.7150/jca.34471.
[49] L. Shen, A. Orillion, R. Pili, Histone deacetylase inhibitors as immunomodulators in cancer therapeutics, Epigenomics 8 (2016) 415–428, https://doi.org/10.2217/epi.15.118.